Supporting Information

Regioselective 5'-Position Phosphorylation of Ribose and Ribonucleosides: Phosphate Transfer in the Activated Pyrophosphate Complex in Gas Phase

Jun Hu, Wen Lei, Jiang Wang, Hong-Yuan Chen, Jing-Juan Xu*

State Key Laboratory of Analytical Chemistry for Life Science, School of Chemistry and Chemical Engineering, Nanjing University, Nanjing 210023, P.R. China.

*To whom correspondence may be addressed. Tel/Fax: +86-25-89687294; E-mail address: xujj@nju.edu.cn.

Contents

Materials and Experiments

Additional Figures

Figure S1. Scanning electron micrographic characterization of the microemitter for nESI.

Figure S2. The tandem mass spectrum of the complex between ribose and phosphate.

Figure S3. The isolation and collisional activation of cationic complexes between SAPP and ribose.

Figure S4. The isomeric identity of the ribose phosphate by tandem mass spectrometric analysis using stable isotope (^{13}C) labeling technology.

Figure S5. Reaction efficiency of the ribose phosphorylating.

Figure S6. Mass spectra from aqueous solution containing a mixture of sugar and SAPP.

Figure S7. Reaction efficiency of sugar phosphorylating with pyrophosphate.

Figure S8. Mass spectra from aqueous solution containing ribonucleoside and SAPP.

Figure S9. Comparison of the tandem mass spectra between common nucleoside phosphates and gas-phase prepared nucleoside phosphates.

Figure S10. Conversion rate of the anionic complex between the ribonucleoside and SAPP.

Figure S11. Formation of ribonucleoside diphosphates.

Figure S12. Comparison of the tandem mass spectra between nucleoside diphosphate standards and gas phase-collision produced nucleoside phosphates.

Figure S13. Conversion rate of the anionic complex between the ribonucleoside and STPP.

Figure S14. Comparison of the tandem mass spectra between common R5P and the gas-phase prepared R5P.

Figure S15. Tandem mass spectra of stable isotope (^{13}C) labeled [R5P -H$_2$O -H]$^-$ ions.

Materials and Experiments

[13]C labeled D-ribose was purchased from IsoReag. All other chemicals were purchased from Sigma Aldrich or Aladdin Reagents. Deionized water was purchased from Wahaha. Glass capillaries (BF100-58-10) were pulled using a micropipette puller (P2000, Sutter Instrument Co.) to create micro emitters with ∼1.5 μm openings. The emitters sputtered with a Pt layer (∼4 nm) were characterized using SEM (Hitachi S-4800 Instrument), see Figure S1. The aqueous solution of 0.1 mM D-ribose (or ribonucleosides), 0.2 mM pyrophosphate was sprayed using a home-built nESI source with micro emitters placed in front of the inlet of the mass spectrometer at a distance of ∼5 mm with a potential of 1.5 kV applied between the emitter and the inlet of the mass spectrometer. The mass spectrometric analysis was carried out using a Q-TOF mass spectrometer (6530B, Agilent) and activation of the electrostatic complex were carried out in the collision cell and a voltage varying from 0 to 30 V was used to accelerate ions for the energetic collision with helium. The instrument parameters were as follows: Gas Temp = 300 °C, Nebulizer = 0 psig, Fragmentor = 135. All other parameters were kept default. A hybrid mass spectrometer (LTQ Orbitrap Velos, Thermo Fisher Scientific) was also used to acquire the ms[3] and ms[4] data with normalized energy of 5∼15 % used. The capillary temperature was 150 °C. The spray voltage was 1.5 kV. All other parameters were kept default. For the calculation of the conversion rate, only data acquired using a Q-TOF mass spectrometer were used as the mass discrimination effect of a LTQ based mass spectrometer in tandem mass spectrometric analysis can cause significant deviation.
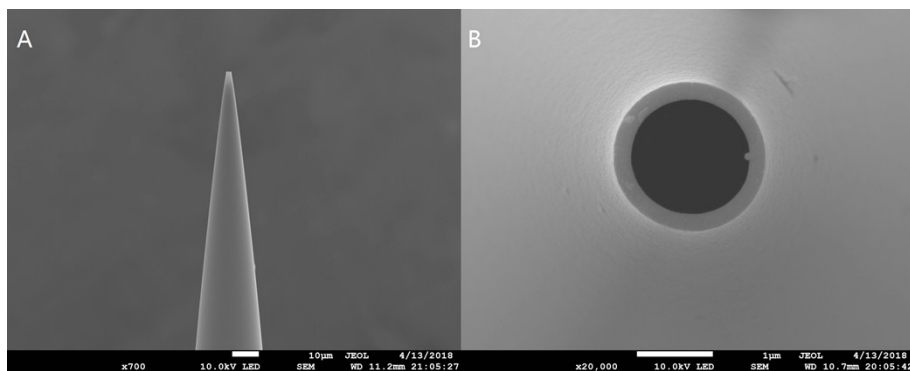
Additional Figures

Figure S1. Scanning electron micrographs of the emitters with a ~1.5 µm opening. (A) horizontal view, (B) vertical view.
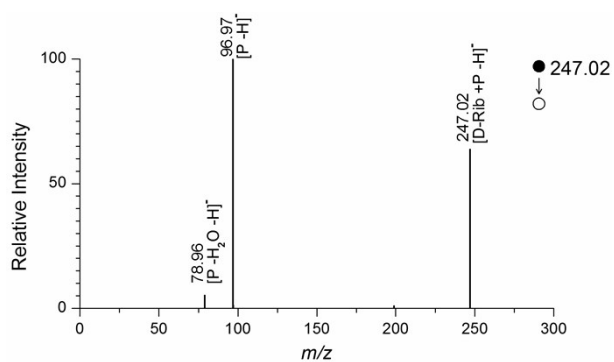

Figure S2. The tandem mass spectrum of the complex between ribose and phosphate.

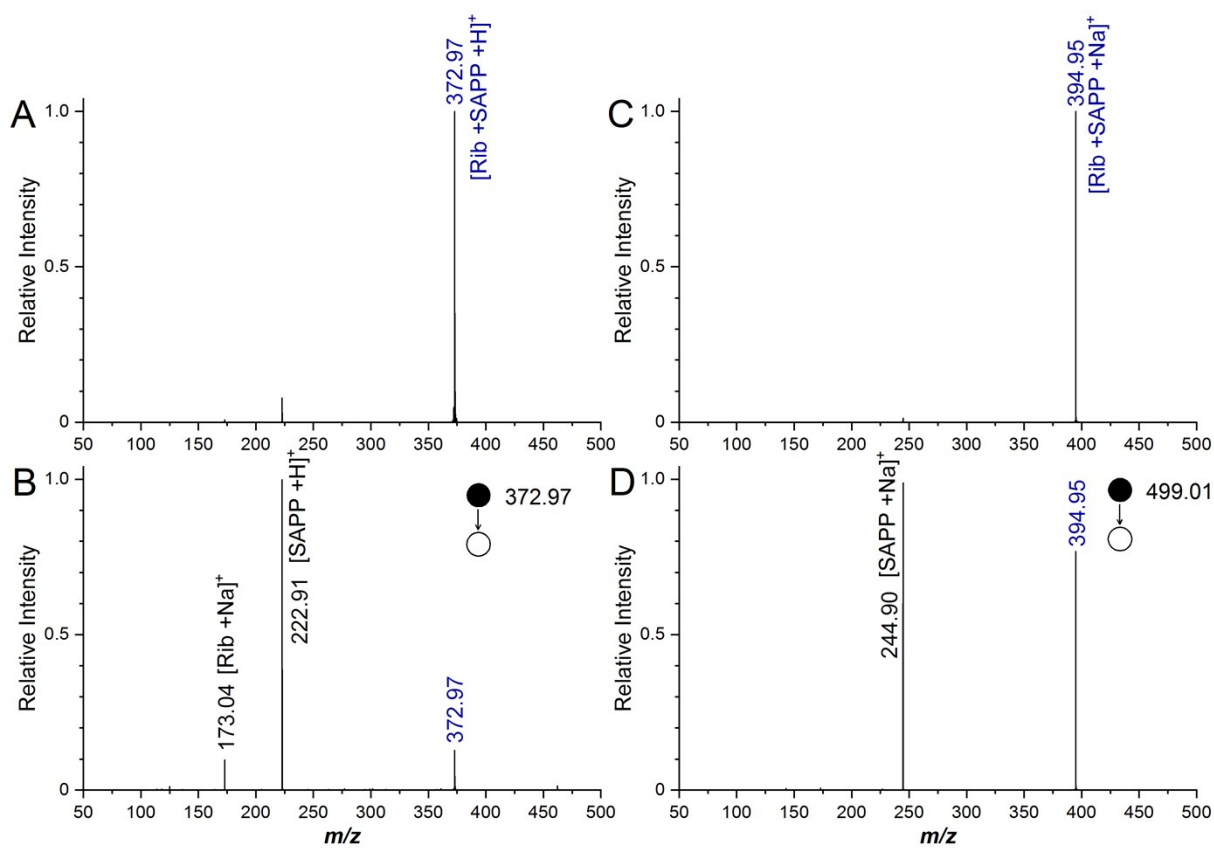**Figure S3**. The isolation of cationic complexes between SAPP and ribose: (A) [Rib +SAPP +H]$^+$ and (C) [Rib +SAPP +Na]$^+$. The activation of cationic complexes between SAPP and ribose: (B) [Rib +SAPP +H]$^+$ and (D) [Rib +SAPP +Na]$^+$.
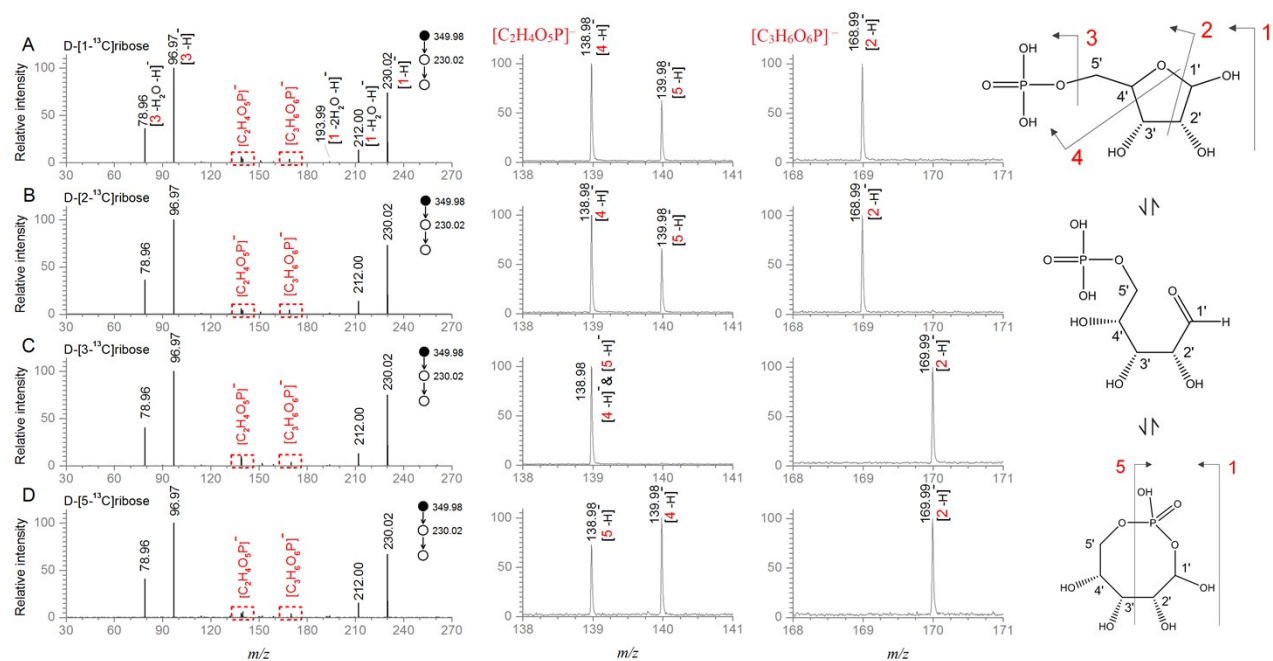
Figure S4. The isomeric identity of the ribose phosphate by tandem mass spectrometric analysis using stable isotope (^{13}C) labeling technology. The tandem mass spectrum of (A) D-[1-^{13}C]ribose phosphate, (B) D-[2-^{13}C]ribose phosphate, (C) D-[3-^{13}C]ribose phosphate, (D) D-[5-^{13}C]ribose phosphate. In the right were the zoomed mass spectra of the daughter ions $[C_2H_4O_5P]^-$ and $[C_3H_6O_6P]^-$, as well as the illustration of the putative fragmentation patterns. The carbon atoms of the ribose are numbered with primes.
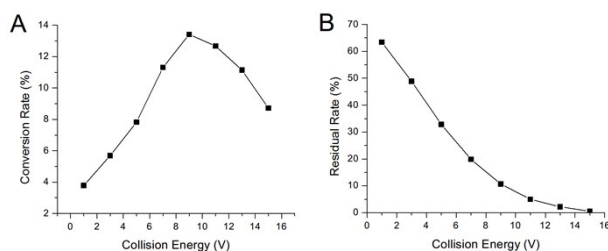

Figure S5. Reaction efficiency of the ribose phosphorylating: (A) conversion rate of ribose-SAPP complex to R5P, (B) residual rate of the complex under varying collision energy.
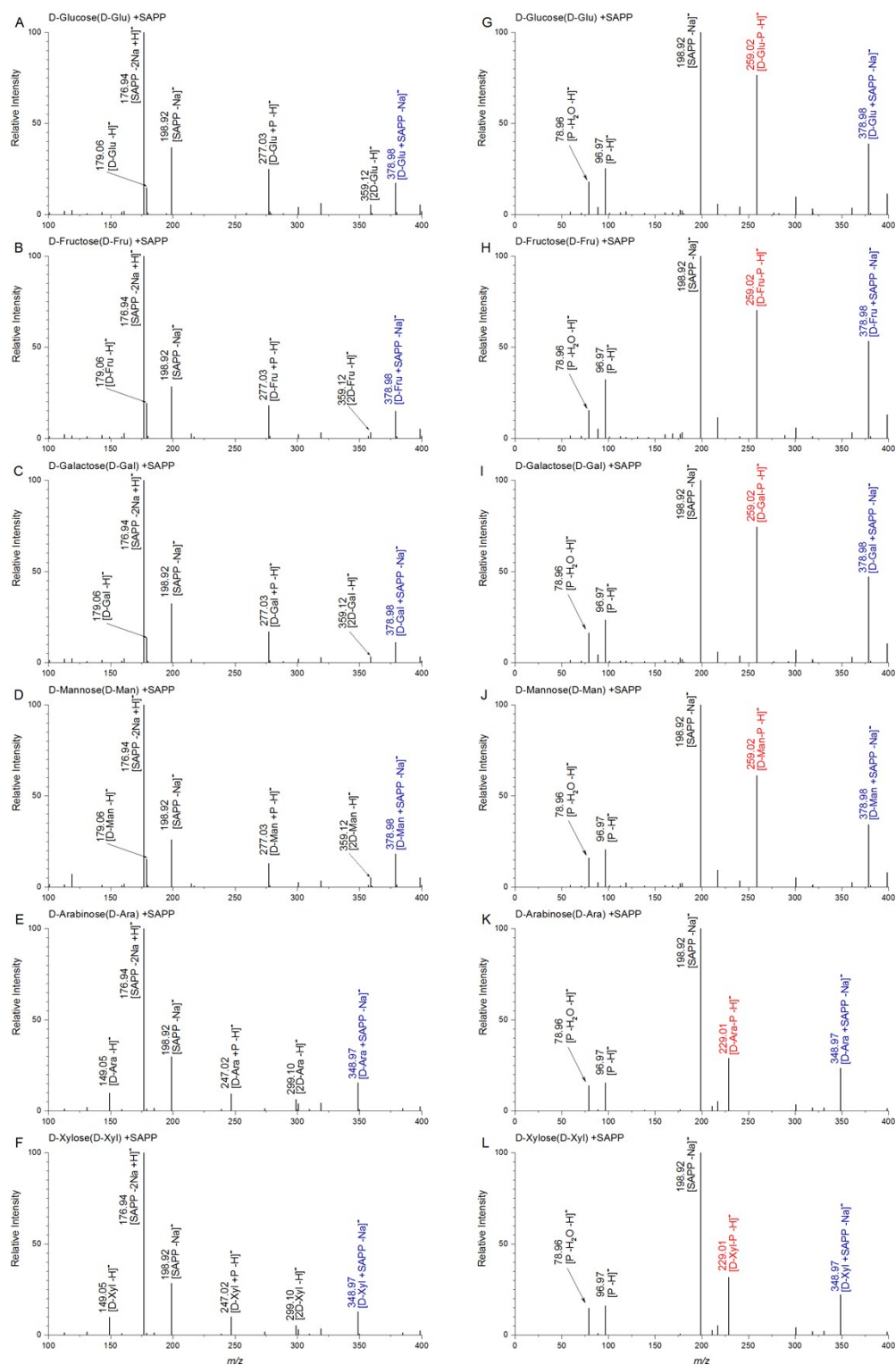
Figure S6. Mass spectra from aqueous solution containing a mixture of sugars and SAPP: (A-F) complexes formation using ESI, (G-L) complexes activation via CID. (A, G) D-Glucose, (B, H) D-Fructose, (C, I) D-Galactose, (D, J) D-Mannose), (E, K) D-Arabinose and (F, L) D-Xylose.
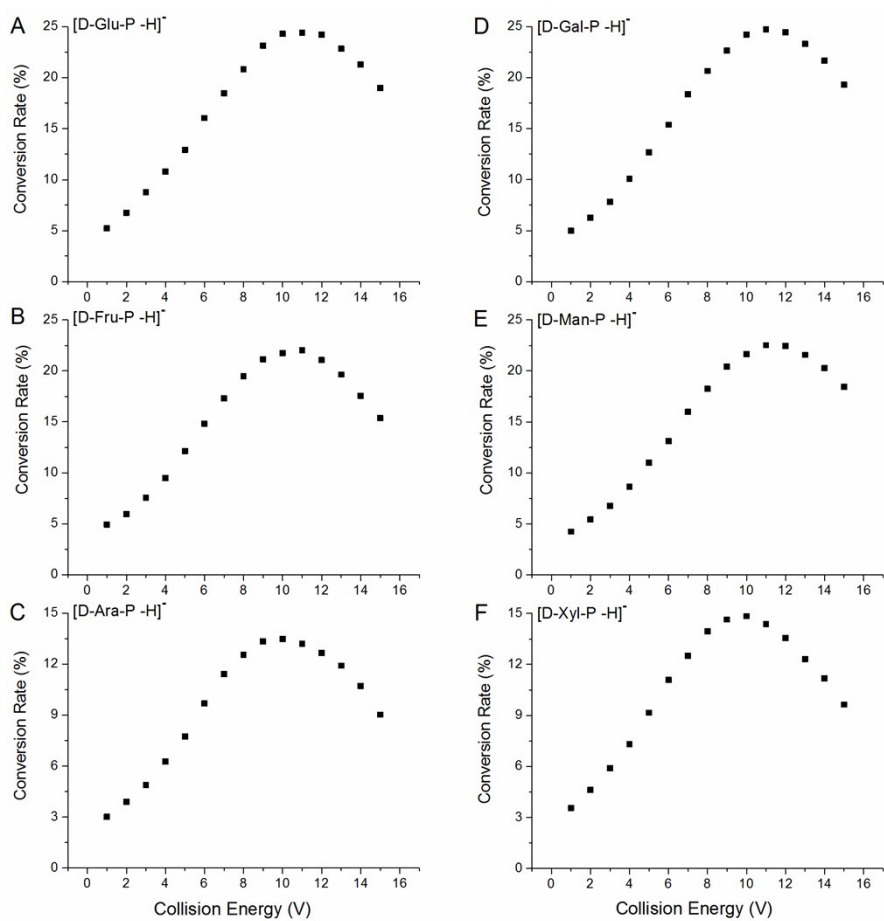
Figure S7. Reaction efficiency of the sugar phosphorylating with pyrophosphate under varying collision energy. Under the optimal collision energy, the conversion efficiency is 24.4 %, 22.0 %, 24.7 %, 22.5 %, 13.5% and 14.8% for (A) D-Glucose, (B) D-Fructose, (C) D-Galactose, (D) D-Mannose), (E) D-Arabinose and (F) D-Xylose, respectively.
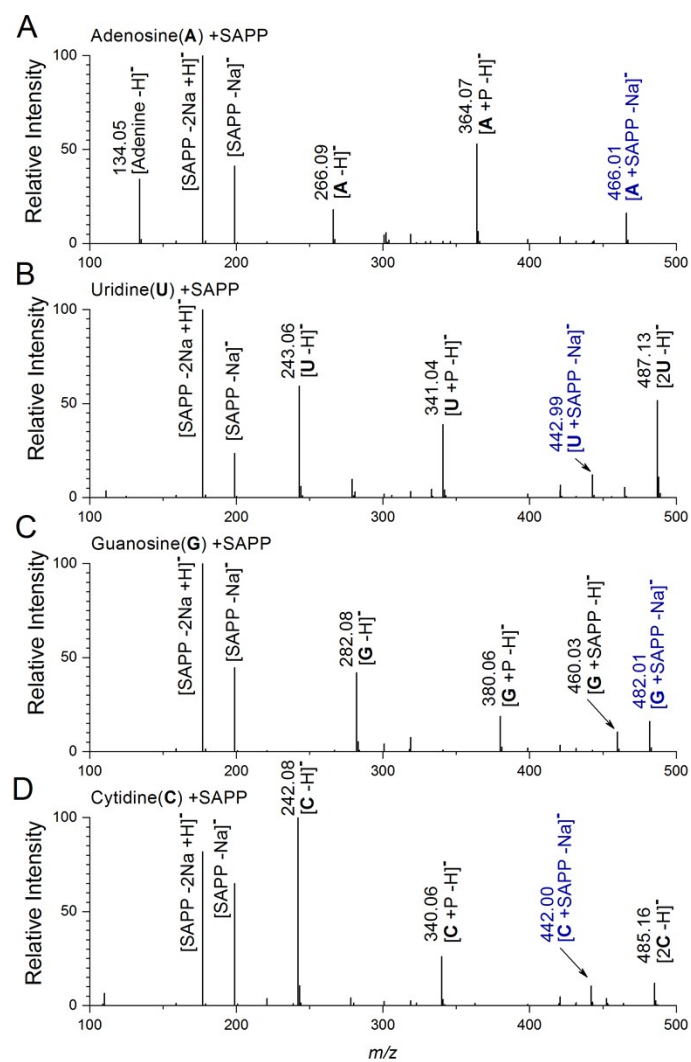
Figure S8. Mass spectra from aqueous solution containing a mixture of 0.1mM ribonucleoside and 0.2 mM SAPP. (A) adenosine, (B) uridine, (C) guanosine and (D) cytidine. The electrostatic complexes between ribonucleosides and SAPP were denoted with blue numbers and letters.
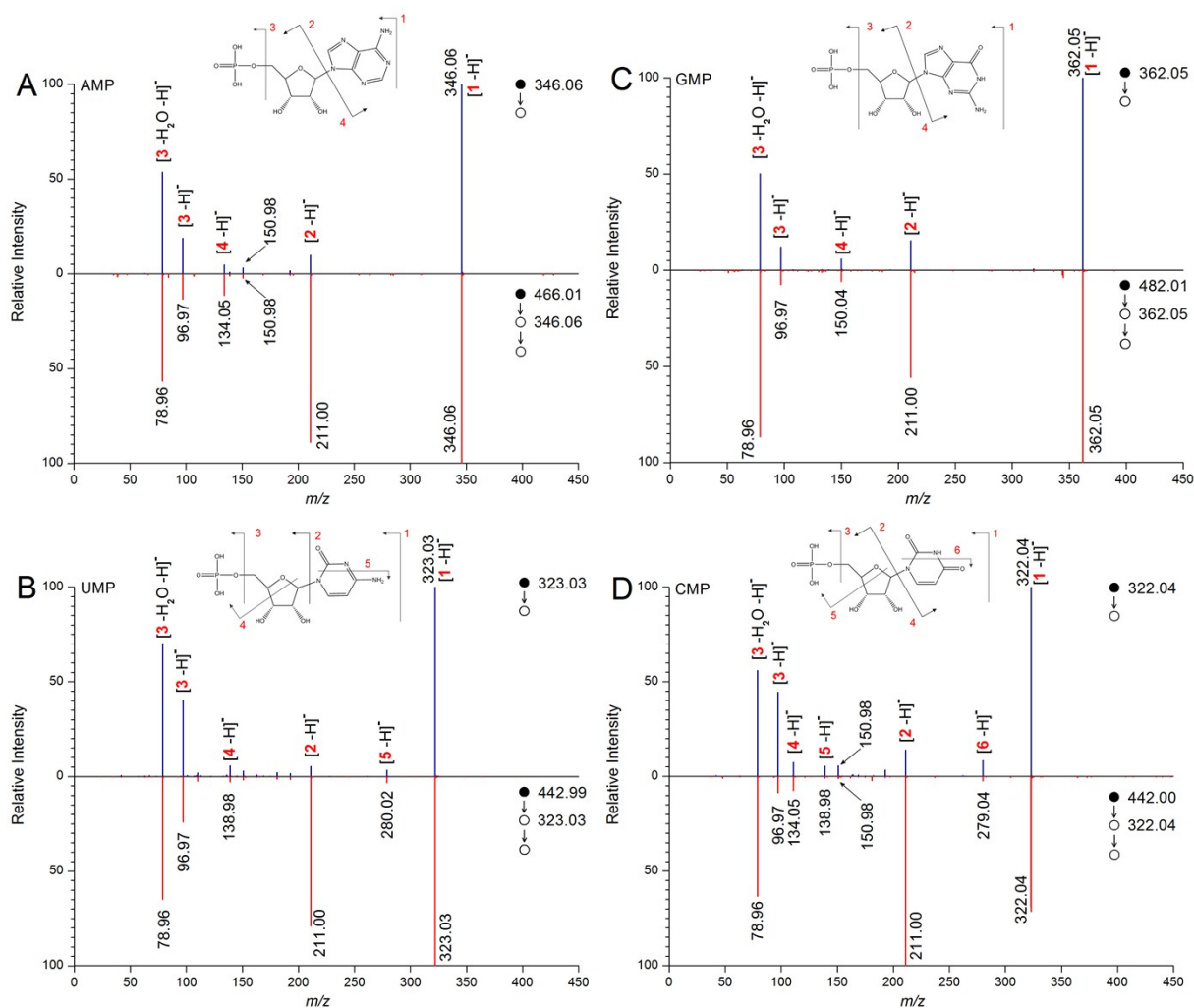
Figure S9. Comparison of the tandem mass spectra between common nucleoside phosphates (curve in blue) and gas phase-collision produced nucleoside phosphates (curve in red). (A) AMP, (B) UMP, (C) GMP and (D) CMP. Inserts were the illustration of the putative fragmentation patterns. Note the peaks at m/z = 211.00 might also be formed through the fragmentation between the C-2 and C-3 of cyclic intramolecular hemiacetal of NMPs, which are similar to that of R5P, see Figure S4 and Figure S15.
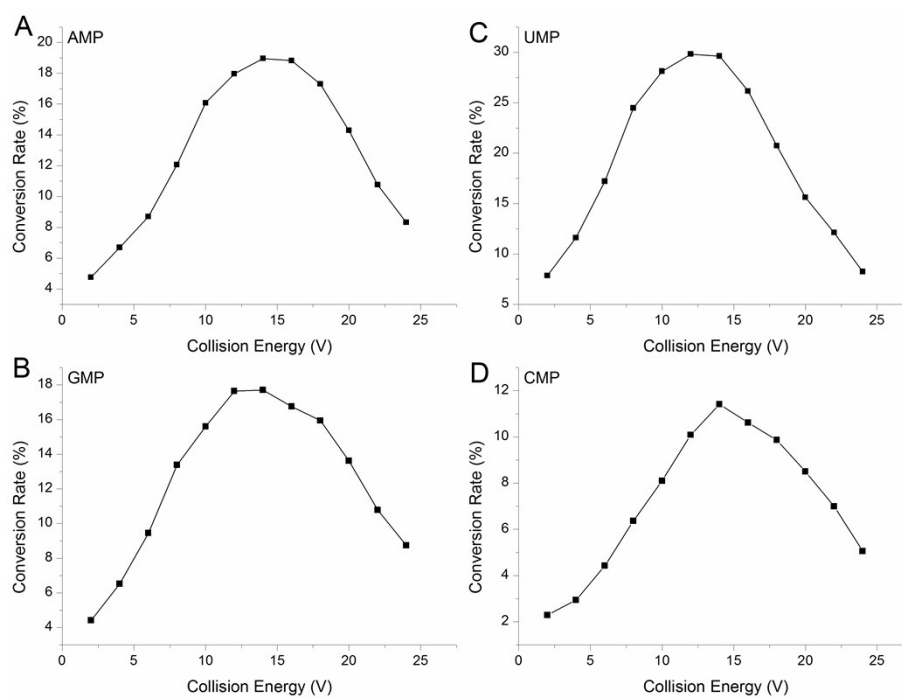
Figure S10. Conversion rate of the anionic complex between the ribonucleoside and SAPP under varying collision energy to produce (A) AMP, (B) GMP, (C) UMP and (D) CMP.
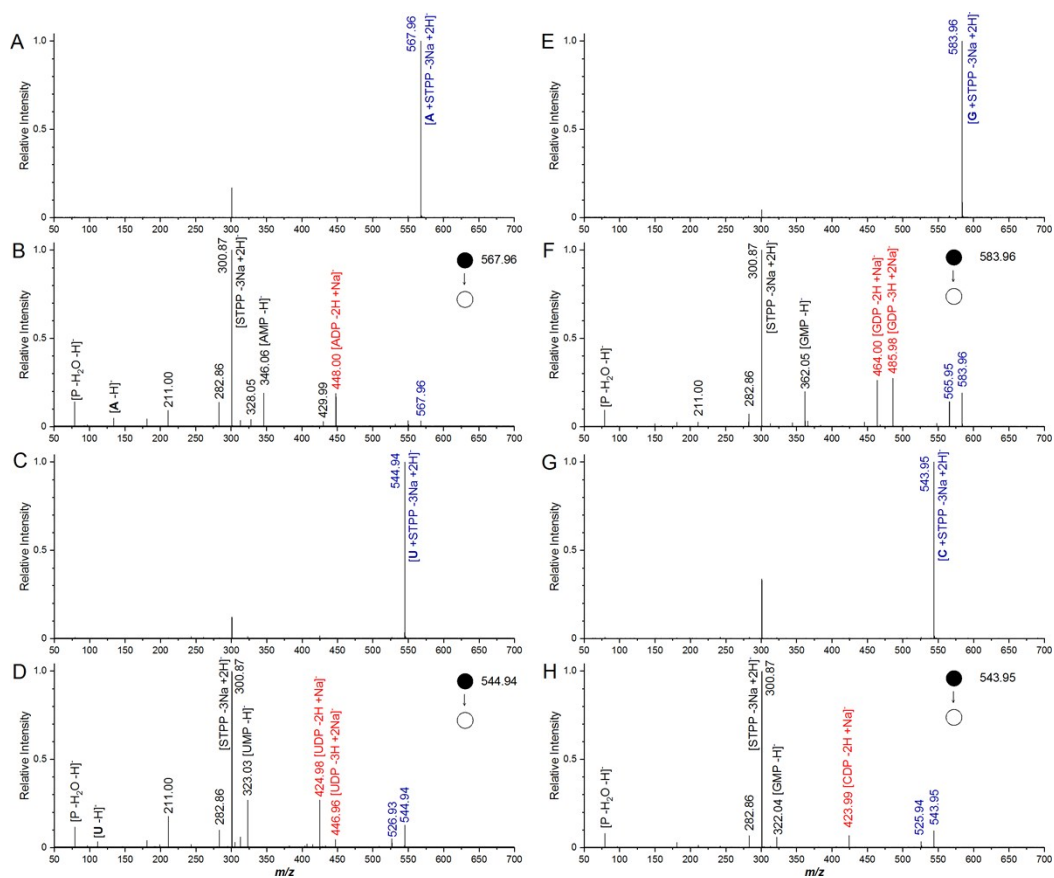
Figure S11. Formation of ribonucleoside diphosphates. The isolation of anion complexes between STPP and ribonucleosides: (A) adenosine, (C) uridine, (E) guanosine and (G) cytidine. The activation of the electrostatic complex via low energy collision to prepare ribonucleoside diphosphates: (B) ADP, (D) UDP, (F) GDP and (H) CDP. The blue numbers and letters denote the anionic complex between ribonucleoside and sodium tripolyphosphate (STPP, $Na_5P_3O_{10}$). The red numbers and letters denote the newly formed ribonucleoside diphosphates. Under the optimal collision energy, the conversion rates for AMP, UDP, GMP and CMP were 5.2 %, 13.1 %, 12.8 and 5.0 %, respectively (see Figure S13).
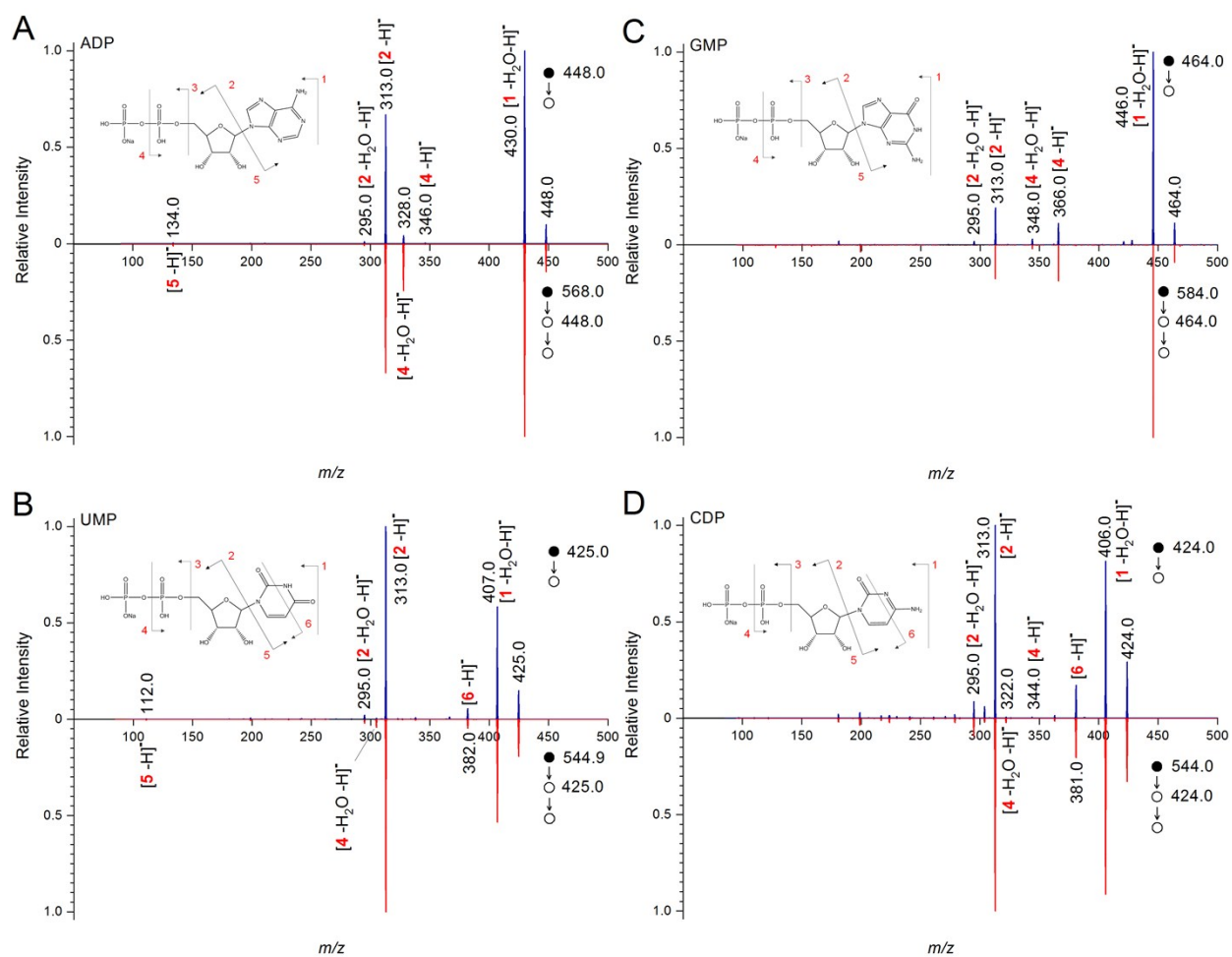
Figure S12. Comparison of the tandem mass spectra between nucleoside diphosphate standards (curve in blue) and gas phase-collision produced nucleoside phosphates (curve in red): (A) ADP, (B) UDP, (C) GDP and (D) CDP. Inserts were the illustration of the putative fragmentation patterns.
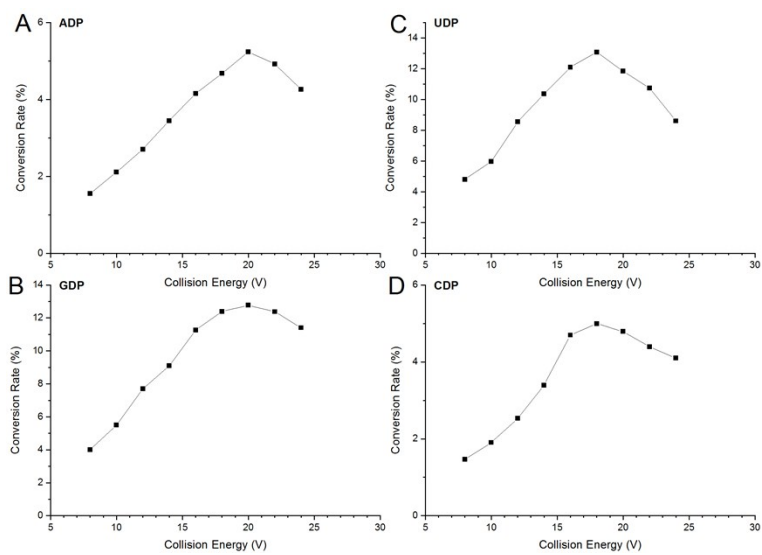
Figure S13. Conversion rate of the anionic complex between the ribonucleoside and STPP under varying collision energy to produce (A) ADP, (B) GDP, (C) UDP and (D) CDP.
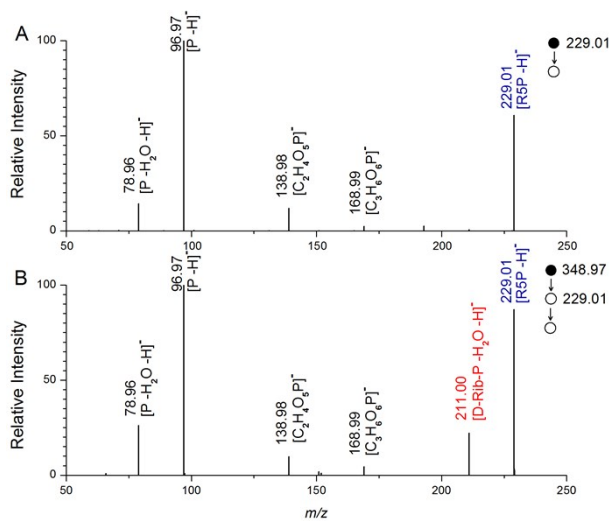
Figure S14. Comparison of the tandem mass spectra between (A) the common R5P and (B) the gas phase-collision prepared R5P. The blue numbers and letters denote the peak of the precursor ion. The red numbers and letters denote the peak at $m/z = 211.00$, which is of a higher relative intensity in comparison with that of the common R5P.
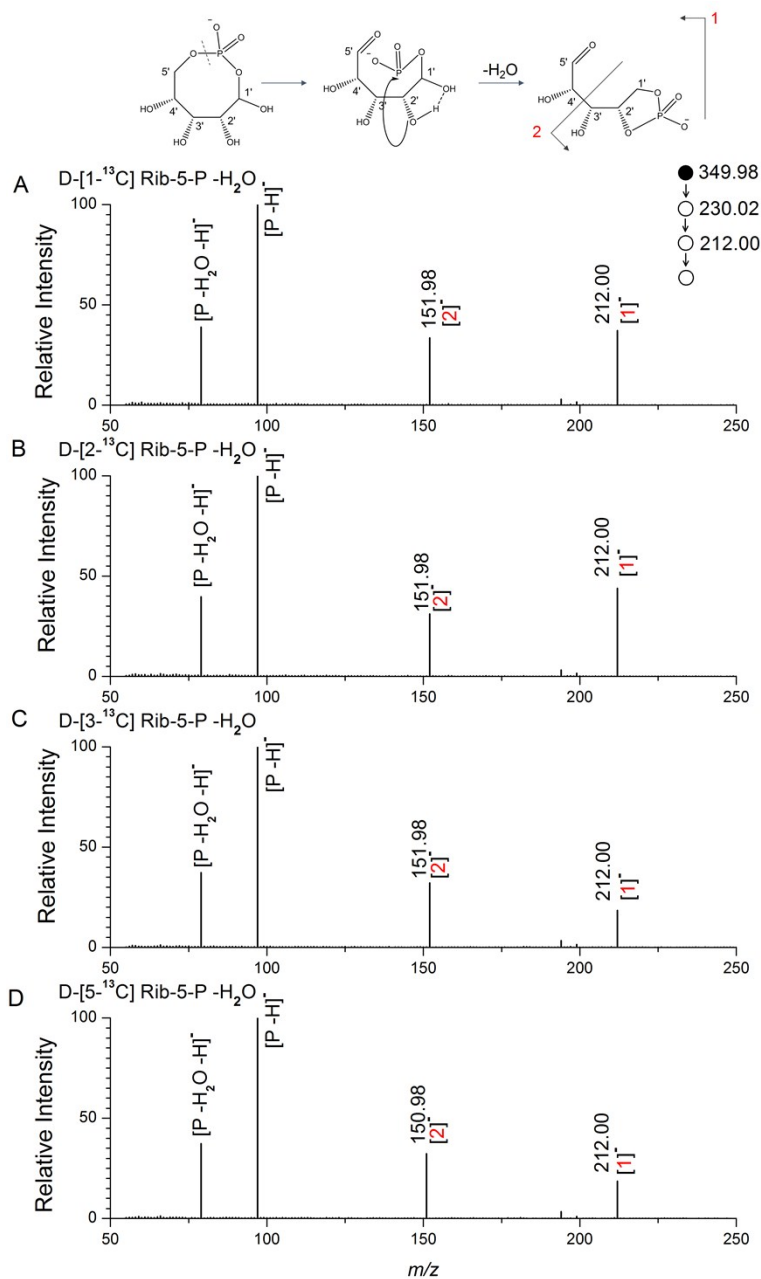
Figure S15. Tandem mass spectra of stable isotope (^{13}C) labeled [R5P -H$_2$O -H]$^-$ ions (A) D-[1-^{13}C]ribose phosphate, (B) D-[2-^{13}C]ribose phosphate, (C) D-[3-^{13}C]ribose phosphate, (D) D-[5-^{13}C]ribose phosphate. The illustrations of the putative intermolecular phosphoryl migration and fragmentation patterns were inserted in the top. The carbon atoms of the ribose are numbered with primes. Note the intensity of peaks at m/z = 150.98 and 151.98 were multiplied by a factor of 10. Note that no m/z shifting of +1 was observed in [2]$^-$ (that is [C$_3$H$_6$O$_6$P]$^-$) from the fragmentation of D-[5-^{13}C]ribose 5-phosphate, which suggested the intermolecular phosphoryl migration.

.